Phase Transition in Protocols Minimizing Work Fluctuations

Alexandre P. Solon and Jordan M. Horowitz
Physics of Living Systems Group, Department of Physics, Massachusetts Institute of Technology, 400 Technology Square, Cambridge, Massachusetts 02139, USA

(Received 29 November 2017; published 4 May 2018)

For two canonical examples of driven mesoscopic systems—a harmonically trapped Brownian particle and a quantum dot—we numerically determine the finite-time protocols that optimize the compromise between the standard deviation and the mean of the dissipated work. In the case of the oscillator, we observe a collection of protocols that smoothly trade off between average work and its fluctuations. However, for the quantum dot, we find that as we shift the weight of our optimization objective from average work to work standard deviation, there is an analog of a first-order phase transition in protocol space: two distinct protocols exchange global optimality with mixed protocols akin to phase coexistence. As a result, the two types of protocols possess qualitatively different properties and remain distinct even in the infinite duration limit: optimal-work-fluctuation protocols never coalesce with the minimal-work protocols, which therefore never become quasistatic.

DOI: 10.1103/PhysRevLett.120.180605

Essential to any well-functioning thermodynamic engine is the rapid and reliable extraction of work at high thermodynamic efficiency. Accomplishing this goal requires both characterizing the optimal finite-time protocols that maximize the work extracted (or minimize the work dissipated) [1–4] and understanding the tradeoff (or lack thereof) with the engine efficiency [5–12]. Arguably, though, large power with high efficiency is only useful when the cycle-to-cycle fluctuations are small. Thus, it is equally important to characterize any tradeoffs with power fluctuations [9,13–15].

One place where universal statements about power fluctuations can be made is in autonomous thermodynamic heat engines—those driven by a constant flow of heat down a temperature gradient. For these stationary engines, the thermodynamic uncertainty relation [16–25] imposes a universal tradeoff between power, power fluctuations, and thermodynamic efficiency [26]. One might hope that such a universal tradeoff exists for nonautonomous thermodynamic engines—driven by cyclic variations of an external parameter. Counterexamples, however, invalidate the naive extension of this prediction [13,27–30].

It thus remains to characterize optimal power fluctuations in driven nonautonomous engines. As a first step, we investigate finite-time thermodynamic processes that attempt to minimize both the work fluctuations and the average dissipated work. Specifically, for two canonical models of driven mesoscopic systems—a harmonically trapped Brownian particle [1] and a quantum dot [3], illustrated in Fig. 1—we numerically determine the collection of protocols that optimize the compromise between the average and standard deviation of the work. Remarkably, for the quantum dot, as we shift the weight of our optimization objective from average work to work standard deviation, we observe the analog of a first-order phase transition, featuring two distinct local minima in protocol space that exchange global optimality and mixed protocols akin to phase coexistence. Looking at protocols of increasing duration, we show that protocols minimizing work fluctuations need not be quasistatic in the infinite time limit, and thus remain out of reach of a linear theory.

Lastly, we adopt here the standard deviation as our metric for the magnitude of work fluctuations, largely because it naturally appears in the thermodynamic uncertainty relation, and near equilibrium it has universal properties [28,31–33]. However, there are other ways to characterize work fluctuations. Integrated squared power

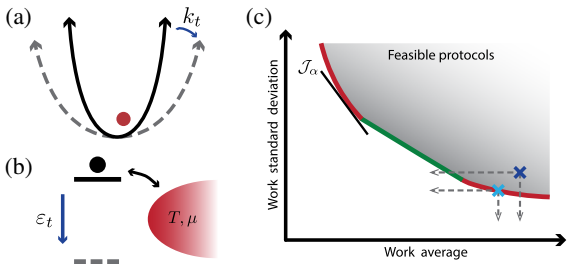

FIG. 1. (a) Harmonically trapped Brownian particle with an expanding spring constant k_t. (b) Quantum dot exchanging particles with a reservoir at temperature T and chemical potential μ with a decreasing energy ε_t. (c) Pareto front (red/green) bounds the region of allowed protocols. A suboptimal protocol (dark blue cross) is dominated by all protocols down and left, including the nondominated protocol (light blue cross). The single objective $\mathcal{J}_\alpha$ is represented by a black line for fixed α, which is optimal when tangent to the front. All solutions along the flat green portion correspond to the same α.

 © 2018 American Physical Society

lends itself to analytic treatment using optimal control theory [34]. Alternatively, single-shot thermodynamics has emerged as a program that allows one to design protocols that make very large fluctuations extremely unlikely [35,36]. Finally, the authors of Ref. [37] have numerically optimized the exponential average of the work.

Setup.—We have in mind a mesoscopic system with states x—continuous or discrete—evolving in a noisy thermal environment at temperature T, under the influence of an externally controlled potential $U(x,\lambda)$. The system is driven by a protocol λ_t during a finite time τ, such that in each realization x_t the work done is $W=\int_0^\tau ds\dot{\lambda}_s\partial_\lambda U(x_s,\lambda_s)$. Due to the noise, the work W is a fluctuating quantity. However, its average $\mu_W[\lambda_t]=\langle W\rangle$ and standard deviation $\sigma_W[\lambda_t]=\sqrt{\langle(W-\mu_W)^2\rangle}$ are uniquely determined by the protocol λ_t. Our goal is then, for fixed protocol duration and end points $(\tau,\lambda_i,\lambda_f)$, to characterize the protocols that minimize either the average work, the standard deviation, or their best compromise.

A general approach to the problem of optimizing a collection of incompatible objectives that cannot be simultaneously optimal—here, μ_W and σ_W—is to utilize the notion of Pareto-optimal solutions in order to classify all the possible optimal protocols [38]. To this end, we will say that a protocol λ_t^1 dominates another, λ_t^2, if it performs better for one of the objectives (i.e., it leads to a smaller μ_W or σ_W) and at least as well in the other objective. The collection of Pareto-optimal protocols—those that are not dominated by any other protocol—form the Pareto front and represent the set of optimal solutions, for which one objective cannot be improved without degrading the other. The Pareto front thus encodes the possible tradeoffs. When plotted in the $\mu_W-\sigma_W$ plane, as in Fig. 1(c), the Pareto-optimal solutions form a boundary to the space of all feasible protocols.

A natural starting point for computing the Pareto front is to minimize a single objective linear function [38]

$$\mathcal{J}_\alpha=\alpha\mu_W+(1-\alpha)\sigma_W, \tag{1}$$

with $\alpha\in[0,1]$. As we vary α from $0\to1$, we shift from minimizing the standard deviation σ_W to minimizing the average work μ_W [39]. As illustrated in Fig. 1(c), a protocol minimizing $\mathcal{J}_\alpha$ is always Pareto optimal. However, the converse need not be true: the family of minima of $\mathcal{J}_\alpha$ maps out the entire Pareto front only if the space of feasible protocols is strictly convex [38]. For example, the green portion of the front in Fig. 1(c) corresponds to a single value of α. In the following, we will encounter both strictly and not strictly convex fronts.

Harmonic trap.—As a first case study, we consider an overdamped Brownian particle in a harmonic trap with potential $U(x,k_t)=k_tx^2/2$, with controllable spring constant k_t. We choose this model for its tractability [5,40,41] and its experimental relevance [42–44]. The particle's dynamics are given by the overdamped Langevin equation

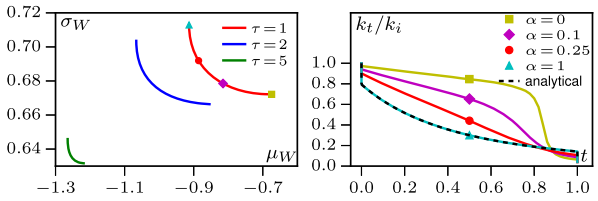

FIG. 2. Left: Pareto front for the harmonic oscillator obtained by minimizing $\mathcal{J}_\alpha$ for three different protocol durations $\tau=1,2,5$. Squares on the $\tau=1$ curve indicate the position of the protocols shown on the right. Right: The optimal protocols deform smoothly along the Pareto front as we vary $\alpha=0\to1$. The dashed black line indicates the exact analytical solution [1]. Both plots are for an expansion $k_f/k_i=0.04$.

$$\gamma\dot{x}_t=-k_tx_t+\sqrt{2\gamma k_BT}\xi_t, \tag{2}$$

where γ is the damping coefficient, T is the temperature, and ξ_t is a zero-mean, Gaussian white noise. We optimize over protocols k_t of fixed duration τ with fixed initial and final values k_i and k_f. Choosing appropriate units, we can take $k_BT=\gamma=1$ and express all results in terms of the ratio k_f/k_i.

Under these constraints, we determine numerically the protocol minimizing $\mathcal{J}_\alpha$ in Eq. (1). This is summarized as follows. (i) Exploiting the linearity of Eq. (2), we derive a closed set of ordinary differential equations (ODEs), whose solution for a given protocol outputs the mean work μ_W and standard deviation σ_W (see Supplemental Material Ref. [45]). (ii) The ODEs are integrated by discretizing the protocol into $N=100$ points with linear interpolations. We also explicitly allow for discontinuities at $t=0$ and $t=\tau$, as these are known to be generic for minimum-work protocols [1,3,4,46,47]. (iii) We then perform a stochastic gradient descent to minimize $\mathcal{J}_\alpha$: At each step, a small trial move δk of one point of the protocol is proposed and accepted if it decreases $\mathcal{J}_\alpha$. Remarkably, the protocol space is found to be very smooth, so that the optimization procedure converges to a unique minimum independently of the initial condition. This was checked for each α using 100 random initial protocols, with each point drawn from a uniform distribution on $[0,2k_f]$.

Repeating the process for different values of α, we obtain the family of solutions shown in Fig. 2 (left) for an expansion with $k_f/k_i=0.04$ and protocol durations $\tau=1$, 2, 5. We observe that when varying α from 0 to 1, the optimal protocols draw a continuous and convex line in the $\mu_W-\sigma_W$ plane, which thus corresponds to the full family of Pareto-optimal solutions. Correspondingly, the optimal protocols, shown in Fig. 2 (right) for $\tau=1$, deform smoothly along the Pareto front. For $\alpha=1$, our algorithm recovers the minimum-work protocol derived analytically in Ref. [1]. This minimum-work protocol smoothly decreases over the entire interval (apart from discontinuous jumps at the edges), whereas the minimum-fluctuation

protocol stays relatively constant before dropping quickly. By keeping the oscillator confined, the small spread in position translates to a small spread in work values during the final rapid expansion, despite costing work (cf. Ref. [9]).

If we focus our attention on the optimal work protocols at $\alpha = 1$, we observe that the Pareto front's asymptote is vertical. This indicates that to reach the optimal work protocol, one must sacrifice a lot of fluctuations, relatively speaking. Put another way, there are many near-optimal protocols with substantially less fluctuation, complementing Ref. [48], which found in a driven Ising model that near-optimal protocols can be numerous. Similarly, the flat asymptote at $\alpha = 0$ near the optimal-work-fluctuation protocol indicates that a lot of dissipation is necessary to reduce the fluctuations to a minimum.

Two-level system.—To allow for more complex behavior, we now optimize a quantum dot [3,49]. We model its dynamics as a Markov jump process with two discrete states: empty or filled with one electron. Jumps between states occur due to the exchange of a particle with a reservoir. We denote by ε_t the difference between the energy level of the dot and the chemical potential of the reservoir. The system is fully characterized by the probability p_t to be filled, which evolves as (see Refs. [3,45])

$$\dot{p}_t = -\omega p_t + \frac{\omega}{1 + e^{\varepsilon_t / k_B T}}, \tag{3}$$

with bare rate constant ω. We choose $\omega = k_B T = 1$, fixing time and energy units.

Like the harmonic oscillator, the linearity of Eq. (3) allows us to construct a set of ODEs whose solution gives μ_W and σ_W for a protocol ε_t changing from ε_i at $t = 0$ to ε_f at τ. The optimization procedure is identical to that of the harmonic trap. We choose here a representative set of parameters $\varepsilon_i = 4$, $\varepsilon_f = -4$, and $\tau = 1$. The protocols minimizing $\mathcal{J}_\alpha$ for $\alpha \in [0, 1]$ are shown in red in Fig. 3(a). Strikingly, as we vary α from 0 to 1, tracing the red line from bottom right to top left, there is a discontinuous break (hopping over the green segment), signaling a jump in protocol space (at $\alpha^* \approx 0.305$ for our parameters). This corresponds to a qualitative change in the optimal protocols pictured in Fig. 3(b)—from minimum-fluctuation-like protocols with ε_t increasing (apart from discontinuous jumps at the end points), to minimum-work-like protocols with ε_t decreasing. The transition happens when these two different solutions that are locally optimal in protocol space exchange global optimality.

The missing portion of the Pareto front can be accessed by optimizing a different function,

$$\mathcal{G}_\mu = \kappa(\mu_W - \mu_0)^2 + \sigma_W, \tag{4}$$

for a fixed value of μ_0. Taking large $\kappa = 10$, the protocol that minimizes $\mathcal{G}_\mu$ has an average work very close to the

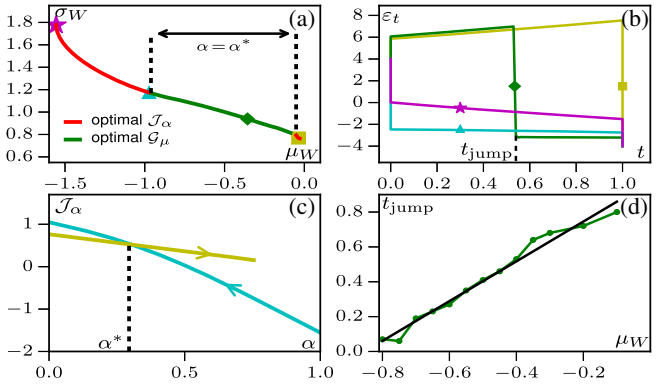

FIG. 3. (a) Pareto front for the quantum dot, obtained by minimizing $\mathcal{J}_\alpha$ and $\mathcal{G}_\mu$. Symbols indicate the positions of the protocols shown in (b). (b) Optimal work protocol (magenta), the two protocols at $\alpha = \alpha^*$ on the minimum-work and mimimum-work-fluctuation branches (blue and yellow), and a protocol in the coexistence region (green). (c) Optimal $\mathcal{J}_\alpha$ obtained by ramping α up (yellow) or down (blue) without restarting from a random initial protocol; the exchanging of global optimality occurs at α^*. (d) Position of the discontinuity in phase-coexistence protocols as a function of μ_W with a linear fit. Parameters: $\tau = 1$, $\varepsilon_i = 4$, $\varepsilon_f = -4$.

fixed value $\mu_W \approx \mu_0$ and minimum standard deviation. It is thus a good approximation of the point on the Pareto front at μ_0. (An alternative method imposing a hard inequality constraint can be found in Ref. [50].) Varying μ_0 then yields the green portion of Fig. 3(a), thereby completing the front. The resulting protocols, as shown in Fig. 3(b), exhibit a sharp jump in the middle. Numerically, we find that in this part of the phase diagram our stochastic gradient descent can get trapped in local minima corresponding to different positions of the jump. To find the global minimum of $\mathcal{G}_\mu$, we thus performed many runs (>500) with different initial conditions to sample all local minima. For more precision, we also adapted our code to replace sharp gradients with exact discontinuities.

Putting everything together, the picture is similar to that of a first-order liquid-gas transition [38]. The parameter α in $\mathcal{J}_\alpha$ plays the role of an intensive parameter (say the pressure), whereas $\mathcal{J}_\alpha$ is analogous to the free energy: There is a finite

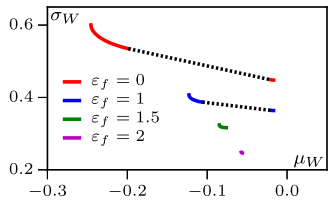

FIG. 4. Pareto front of the quantum dot for varying ε_f at fixed $\varepsilon_i = 4$ and $\tau = 1$. For $\varepsilon_f > 1$, the optimal-work-fluctuation solution family disappears, and the Pareto front becomes strictly convex. Dotted black lines are guides to the eye denoting the coexistence regions.

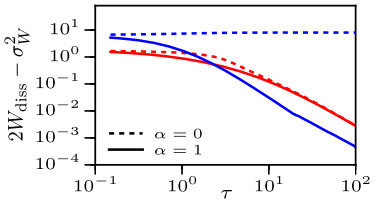

FIG. 5. Approach to the linear-perturbation regime for optimal work and work-fluctuation protocols as τ increases. Harmonic oscillator (red lines) with $k_f/k_i = 0.04$ and quantum dot (blue lines) with $\varepsilon_i = 4$, $\varepsilon_f = -4$.

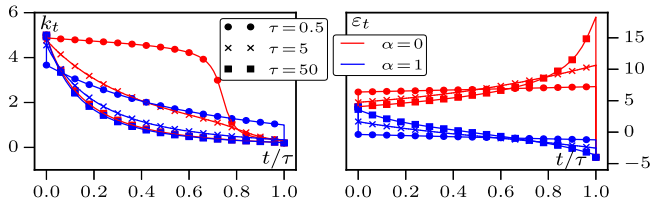

FIG. 6. Optimal-work ($\alpha = 1$) and work-fluctuation ($\alpha = 0$) protocols of varying duration τ. Left: Harmonic oscillator with $k_f/k_i = 0.04$. The two protocols become identical in the large-duration limit. Right: Quantum dot with $\varepsilon_i = 4$, $\varepsilon_f = -4$. The two protocols remain different for large durations.

jump to a different protocol at a critical α^* where the two solutions exchange global optimality. As in a liquid-gas transition, these "homogeneous" solutions remain metastable beyond α^*. Although these suboptimal solutions are not part of the Pareto front, they can be accessed by slowly ramping α while minimizing $\mathcal{J}_\alpha$ without restarting from a random initial protocol, in the same way that hysteresis loops are observed by ramping fluid pressure. The transition point α^* corresponds to the exchange of global optimality, as shown in Fig. 3(c).

Minimizing $\mathcal{G}_\mu$ is then akin to switching to a constant-volume (canonical) ensemble. This allows us to observe the analog of phase coexistence *inside* the protocols: One observes a family of protocols (all at $\alpha = \alpha^*$) that comprise two parts—decreasing minimum-work-like and increasing minimum-fluctuation-like protocols—linked together by a discontinuity. As shown in Fig. 3(d), the proportions of each "phase" vary linearly along the front (up to numerical uncertainty), similar to what the lever rule predicts for a liquid-gas transition.

The two "homogeneous" solutions correspond to two distinct strategies: (i) The optimal work is achieved by monotonically decreasing the energy level, while (ii) the minimum standard deviation is achieved by first increasing the energy to confine the system into a single discrete state with almost no spread in state space prior to a rapid fluctuationless switch. Physically, in case (i), the dot is partially filled, and the protocol tries to keep the distribution as much like the equilibrium distribution as possible. In case (ii), the dot is mostly empty, and thus it ends with a distribution very different from the final equilibrium. The trapping of the distribution, made possible by the system's discreteness, is at the origin of the transition. This is confirmed by Fig. 4, which shows the Pareto fronts for different ε_f at fixed $\varepsilon_i = 4$. For larger $\varepsilon_f > 1$, the initial and final energy levels are not separated enough to make the compressed distribution very different from the final equilibrium. Consequently, the optimal protocols approach the linear regime where work fluctuations are constrained to be equal to the average work [2,31], forcing the optimal-work-fluctuation branch to disappear.

Quasistatic limit.—This disappearance of the transition suggests a similar phenomenon would occur for the linear regime reached for long times [12,51–56]. Thus, we would expect all optimal protocols to collapse onto a quasistatic one that remains nearly in equilibrium at every point in time. The second law of thermodynamics, however, only guarantees that minimum-work protocols will become quasistatic, whereas this need not be true for protocols optimizing a different quantity. Indeed, we show here that the protocols minimizing work fluctuations for the quantum dot never become quasistatic.

Close to the quasistatic limit, linear response predicts that $2W_{\rm diss} = \sigma_W^2$, with $W_{\rm diss} = \mu_W - \Delta F$ being the dissipated work and ΔF the free-energy difference between the initial and final equilibria [31,33]. For the harmonic oscillator, Fig. 5 shows that as τ increases, the linear response regime is approached by both the optimal-work and optimal-work-fluctuation protocols. On the contrary, for the quantum dot, only the optimal-work protocol approaches the linear regime. Even in the infinite-time limit, the optimal-work-fluctuation protocol dissipates a finite amount and thus remains nonquasistatic.

The different limits are best understood by looking at how the optimal protocols change as τ increases, as shown in Fig. 6. For the harmonic oscillator, the whole Pareto front contracts to a point in protocol space as the two extremities for $\alpha = 0$ and $\alpha = 1$ converge to the same protocol. On the contrary, the protocols corresponding to minimal mean work and work standard deviation remain different as $\tau \to \infty$ for the quantum dot. The structure of the phase diagram of Fig. 3 is preserved upon increasing τ so that there always exist two "phases." Only the family containing the optimal-work protocol becomes quasistatic for large τ, while the optimal-fluctuation protocols retain instantaneous jumps and are therefore not quasistatic. Thus, studies of optimal-work-fluctuation protocols within linear irreversible thermodynamics cannot access the optimal solution.

To summarize, we have shown that for the harmonic oscillator, the tradeoff between work and work fluctuations is captured by a smooth family of protocols. However, this behavior is not generic. For a quantum dot, approximating a double-well potential, optimal-work and work-fluctuation protocols belong to qualitatively different "phases." The tradeoffs between the two, captured by the Pareto front,

have the structure of a first-order phase transition with phase-coexistence protocols interpolating between the two phases. Such a phase transition may be a common feature of optimization problems: they occur in optimal complex networks [57,58] and statistical inference [59], and similar phenomena were observed in a quantum control problem with varying constraints [60] and in the utilization of memory in an information engine [61–63]. Finally, we observed that the minimum-work fluctuation and the phase-coexistence protocols do not become quasistatic even for very long protocols and are thus not accessible by a linear theory.

We are especially grateful to Todd R. Gingrich and Luis F. Seoane for their advice and suggestions, and we acknowledge the Gordon and Betty Moore Foundation for supporting us as Physics of Living Systems Fellows through Grant No. GBMF4513.

[1] T. Schmiedl and U. Seifert, Optimal Finite-Time Processes in Stochastic Thermodynamics, Phys. Rev. Lett. **98**, 108301 (2007).
[2] H. Then and A. Engel, Computing the optimal protocol for finite-time processes in stochastic thermodynamics, Phys. Rev. E **77**, 041105 (2008).
[3] M. Esposito, R. Kawai, K. Lindenberg, and C. Van den Broeck, Finite-time thermodynamics for a single-level quantum dot, Europhys. Lett. **89**, 20003 (2010).
[4] E. Aurell, C. Mejía-Monasterio, and P. Muratore-Ginanneschi, Optimal Protocols and Optimal Transport in Stochastic Thermodynamics, Phys. Rev. Lett. **106**, 250601 (2011).
[5] T. Schmiedl and U. Seifert, Efficiency at maximum power: An analytically solvable model for stochastic heat engines, Europhys. Lett. **81**, 20003 (2008).
[6] P. Chvosta, M. Einax, V. Holubec, A. Ryabov, and P. Maass, Energetics and performance of a microscopic heat engine based on exact calculations of work and heat distributions, J. Stat. Mech.: Theory Exp. **2010**, P03002 (2010).
[7] M. Moreau, B. Gaveau, and L. S. Schulman, Efficiency of a thermodynamic motor at maximum power, Phys. Rev. E **85**, 021129 (2012).
[8] A. E. Allahverdyan, K. V. Hovhannisyan, A. V. Melkikh, and S. G. Gevorkian, Carnot Cycle at Finite Power: Attainability of Maximal Efficiency, Phys. Rev. Lett. **111**, 050601 (2013).
[9] V. Holubec, An exactly solvable model of a stochastic heat engine: optimization of power, power fluctuations and efficiency, J. Stat. Mech.: Theory Exp. **2014**, P05022 (2014).
[10] N. Shiraishi, K. Saito, and H. Tasaki, Universal Trade-Off Relation between Power and Efficiency for Heat Engines, Phys. Rev. Lett. **117**, 190601 (2016).
[11] O. Raz, Y. Subasi, and R. Pugatch, Geometric Heat Engines Featuring Power that Grows with Efficiency, Phys. Rev. Lett. **116**, 160601 (2016).
[12] K. Proesmans, B. Cleuren, and C. Van den Broeck, Power-Efficiency-Dissipation Relations in Linear Thermodynamics, Phys. Rev. Lett. **116**, 220601 (2016).
[13] F. Ritort, Work and heat fluctuations in two-state systems: A trajectory thermodynamics formalism, J. Stat. Mech.: Theory Exp. **2004**, P10016 (2004).
[14] K. Funo and M. Ueda, Work Fluctuation-Dissipation Trade-Off in Heat Engines, Phys. Rev. Lett. **115**, 260601 (2015).
[15] V. Holubec and A. Ryabov, Diverging, but negligible power at Carnot efficiency: Theory and experiment, Phys. Rev. E **96**, 062107 (2017).
[16] A. C. Barato and U. Seifert, Thermodynamic Uncertainty Relation for Biomolecular Processes, Phys. Rev. Lett. **114**, 158101 (2015).
[17] P. Pietzonka, A. C. Barato, and U. Seifert, Universal bounds on current fluctuations, Phys. Rev. E **93**, 052145 (2016).
[18] P. Pietzonka, F. Ritort, and U. Seifert, Finite-time generalization of the thermodynamic uncertainty relation, Phys. Rev. E **96**, 012101 (2017).
[19] P. Pietzonka, A. C. Barato, and U. Seifert, Affinity- and topology-dependent bound on current fluctuations, J. Phys. A **49**, 34LT01 (2016).
[20] T. R. Gingrich, J. M. Horowitz, N. Perunov, and J. L. England, Dissipation Bounds All Steady-State Current Fluctuations, Phys. Rev. Lett. **116**, 120601 (2016).
[21] T. R. Gingrich, G. M. Rotskoff, and J. M. Horowitz, Inferring dissipation from current fluctuations, J. Phys. A **50**, 184004 (2017).
[22] T. R. Gingrich and J. M. Horowitz, Fundamental Bounds on First Passage Time Fluctuations for Currents, Phys. Rev. Lett. **119**, 170601 (2017).
[23] J. M. Horowitz and T. R. Gingrich, Proof of the finite-time thermodynamic uncertainty relation for steady-state currents, Phys. Rev. E **96**, 020103(R) (2017).
[24] A. Dechant and S.-I. Sasa, Current fluctuations and transport efficiency for general Langevin systems, arXiv:1708.08653v1.
[25] C. Nardini and H. Touchette, Process interpretation of current entropic bounds, Eur. Phys. J. B **91**, 16 (2018).
[26] P. Pietzonka and U. Seifert, Universal trade-off between power, efficiency and constancy in steady-state heat engines, arXiv:1705.05817.
[27] A. C. Barato and U. Seifert, Cost and Precision of Brownian Clocks, Phys. Rev. X **6**, 041053 (2016).
[28] S. Pigolotti, I. Neri, É. Roldán, and F. Jülicher, Generic Properties of Stochastic Entropy Production, Phys. Rev. Lett. **119**, 140604 (2017).
[29] K. Proesmans and C. Van den Broeck, Discrete-time thermodynamic uncertainty relation, Europhys. Lett. **119**, 20001 (2017).
[30] D. Chiuchiù and S. Pigolotti, Mapping of uncertainty relations between continuous and discrete time, Phys. Rev. E **97**, 032109 (2018).
[31] J. Hermans, Simple analysis of noise and hysteresis in (slow-growth) free energy simulations, J. Phys. Chem. **95**, 9029 (1991).
[32] C. Jarzynski, Nonequilibrium Equality for Free Energy Differences, Phys. Rev. Lett. **78**, 2690 (1997).
[33] T. Speck and U. Seifert, Distribution of work in isothermal nonequilibrium process, Phys. Rev. E **70**, 066112 (2004).

[34] R. Filliger and M.-O. Hongler, Relative entropy and efficiency measure for diffusion-mediated transport processes, J. Phys. A **38**, 1247 (2005).
[35] J. Aberg, Truly work-like work extraction via a single-shot analysis, Nat. Commmun. **4**, 1925 (2013).
[36] N. Y. Halpern, A. J. P. Garner, O. C. O. Dahlsten, and V. Vedral, Introducing one-shot work into fluctuation relations, New J. Phys. **17**, 095003 (2015).
[37] G. Xiao and J. Gong, Suppression of work fluctuations by optimal control: An approach based on Jarzynski's equality, Phys. Rev. E **90**, 052132 (2014).
[38] L. F. F Seoane and R. Solé, Multiobjective optimization and phase transitions, in *Proceedings of ECCS 2014* (Springer, New York, 2016), pp. 259–270.
[39] We choose to use the standard deviation σ_w so that all quantities in $\dot{\mathcal{L}}_a$ have the same dimension, although this is not necessary and using the variance σ_w^2 instead would yield the same results.
[40] A. Imparato, L. Peliti, G. Pesce, G. Rusciano, and A. Sasso, Work and heat probability distribution of an optically driven Brownian particle: Theory and experiments, Phys. Rev. E **76**, 050101(R) (2007).
[41] J. M. Horowitz and C. Jarzynski, Illustrative example of the relationship between dissipation and relative entropy, Phys. Rev. E **79**, 021106 (2009).
[42] V. Blickle and C. Bechinger, Realization of a micrometre-sized stochastic heat engine, Nat. Phys. **8**, 143 (2012).
[43] I. A. Martinez, É. Roldán, L. Dinis, D. Petrox, J. M. R. Parrondo, and R. A. Rica, Brownian Carnot engine, Nat. Phys. **12**, 67 (2016).
[44] I. A. Martinez, A. Petrosyan, D. Gueéry-Odelin, E. Trizac, and S. Ciliberto, Engineered swift equilibration of a Brownian particle, Nat. Phys. **12**, 843 (2016).
[45] See Supplemental Material at http://link.aps.org/supplemental/10.1103/PhysRevLett.120.180605 for details of the models and numerical procedure.
[46] A. Gomez-Marin, T. Schmiedl, and U. Seifert, Optimal protocols for minimal work processes in underdamped stochastic thermodynamics, J. Chem. Phys. **129**, 024114 (2008).
[47] E. Aurell, C. Mejía-Monasterio, and P. Muratore-Ginanneschi, Boundary layers in stochastic thermodynamics, Phys. Rev. E **85**, 020103(R) (2012).
[48] T. R. Gingrich, G. M. Rostkoff, G. E. Crooks, and P. L. Geissler, Near-optimal protocols in cimplex nonequilibrium transformations, Proc. Natl. Acad. Sci. U.S.A. **113**, 10263 (2016).
[49] M. Gopalkrishnan, A cost/speed/reliability tradeoff to erasing, Entropy **18**, 165 (2016).
[50] E. Zitzler, Ph.D. thesis, Universität of Zürich, 1999.
[51] S. Rahav, J. Horowitz, and C. Jarzynski, Directed Flow in Nonadiabatic Stocahstic Pumps, Phys. Rev. Lett. **101**, 140602 (2008).
[52] J. M. Horowitz and C. Jarzynski, Exact formula for currents in strongly pumped diffusive systems, J. Stat. Phys. **136**, 917 (2009).
[53] P. R. Zulkowski, D. A. Sivak, G. E. Crooks, and M. R. DeWeese, Geometry of thermodynamic control, Phys. Rev. E **86**, 041148 (2012).
[54] D. A. Sivak and G. E. Crooks, Thermodynamic Metrics and Optimal Paths, Phys. Rev. Lett. **108**, 190602 (2012).
[55] K. Brandner, K. Saito, and U. Seifert, Thermodynamics of Micro- and Nano-systems Driven by Periodic Temperature Variations, Phys. Rev. X **5**, 031019 (2015).
[56] G. M. Rotskoff, G. E. Crooks, and E. Vanden-Eijnden, Geometric approach to optimal nonequilibirum control: Minimizing dissipation in nanomagnetic spin systems, Phys. Rev. E **95**, 012148 (2017).
[57] L. F. Seoane and R. Solé, Phase transitions in Pareto optimal complex networks, Phys. Rev. E **92**, 032807 (2015).
[58] L. F. Seoane and R. Solé, Systems poised to criticality through Pareto selective forces, arXiv:1510.08697.
[59] L. Zdeborová and F. Krzakala, Statistical physics of inference: Thresholds and algorithms, Adv. Phys. **65**, 453 (2016).
[60] M. Bukov, A. G. R. Day, D. Sels, P. Weinberg, A. Polkovnikov, and P. Mehta, Reinforcement learning in different phases of quantum control, arXiv:1705.00565.
[61] D. Hartich, A. C. C Barato, and U. Seifert, Stochastic thermodynamics of bipartite systems: Transfer entropy inequalities and a Maxwell's demon interpretation, J. Stat. Mech.: Theory Exp. **2014**, P02016 (2014).
[62] J. Bechhoefer, Hidden Markov models for stochastic thermodynamics, New J. Phys. **17**, 075003 (2015).
[63] E. Lathouwers and J. Bechhoefer, When memory pays: Discord in hidden Markov models, Phys. Rev. E **95**, 062144 (2017).